PROCEEDINGS OF THE ROYAL SOCIETY A

Proc. R. Soc. A (2007) **463**, 3055–3071
doi:10.1098/rspa.2007.0051
Published online 4 September 2007

Focused tsunami waves

By M. V. Berry

H. H. Wills Physics Laboratory, Tyndall Avenue, Bristol BS8 1TL, UK

Shallower regions in the oceans can act as lenses, focusing the energy of tsunamis, typically onto cusp points where two caustic lines meet. Diffraction theory enables calculation of the profile of a tsunami wave propagating through a cusp. The wave elevation depends on position, time and two main parameters M and B: the large parameter M is the distance of the cusp from the lens, divided by the local wavelength of the tsunami without focusing, and B quantifies the spatial extent of the initial disturbance. Focusing amplifies the wave by a factor A proportional to $M^{1/4}$ and can potentially multiply the tsunami energy (proportional to A^2) 10-fold over a transverse range of tens of kilometres.

Keywords: diffraction; caustics; water waves; ocean

1. Introduction

Tsunamis (Synolakis & Bernard 2006) are long waves on the surface of shallow water (Lamb 1932; Jeffreys & Jeffreys 1956), which can propagate far from an underwater source. On an ocean of constant depth H, the front travels with a speed

$$v = \sqrt{gH} \tag{1.1}$$

(e.g. approx. 700 km h^{-1} for H=4 km). For varying depth $h(\boldsymbol{r})$, the changing speed corresponds to a refractive index proportional to $1/\sqrt{h(\boldsymbol{r})}$. This is higher where the ocean is shallower, so such regions (corresponding, for example, to underwater ridges or islands) can act as lenses (figure 1), focusing the tsunami energy and hence increasing its destructive potential.

My purpose here is to provide an analytical description of the form of the tsunami wave in typical focal regions in the open ocean, i.e. away from coasts. The theory is complicated by three effects. The first is dispersion: waves of wavevector $\boldsymbol{k}$, representing Fourier components of the initial disturbance, have frequency depending on the magnitude $k=|\boldsymbol{k}|$ according to (Lamb 1932)

$$\omega(\boldsymbol{k},\boldsymbol{r}) = \sqrt{gk\tanh(h(\boldsymbol{r})k)} = k\sqrt{gh(\boldsymbol{r})}\left(1-\frac{1}{6}(h(\boldsymbol{r})k)^2\ldots\right), \tag{1.2}$$

where, in the long-wave approximation appropriate to tsunami propagation, only linear and cubic terms need be retained. This dispersion relation assumes small surface elevations on an incompressible, inviscid, irrotational flow.

Dedicated to the memory of Professor D. H. Peregrine.

Received 25 May 2007
Accepted 13 August 2007

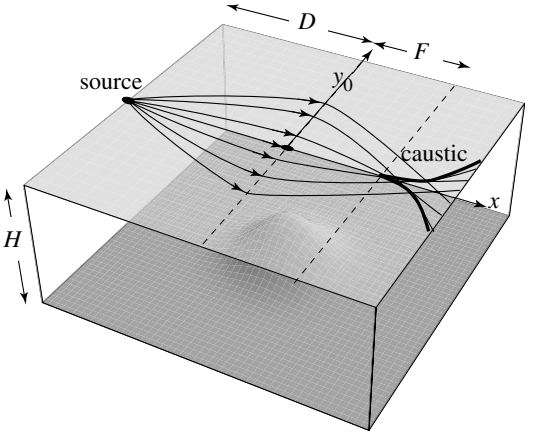

Figure 1. Caustic of tsunami focused by an underwater island 'lens'.

Table 1. Numerical estimates for three different tsunamis, specified by the radius R and height H_i of the island lens and the distance D and size W of initial disturbance; from these quantities are calculated: local wavelength Λ of tsunami arriving at lens, focal distance F, aberration parameter γ, diffraction parameter M, source size parameter B, focusing amplification A and transverse extent Δy of strong focusing. All distances are in kilometres and ocean depth $H=4$ km in all cases.

	R	H_i	D	W	Λ	F	γ	M	B	A	Δy
a	500	2	2000	10	96	786	0.66	28	0.13	3.37	88
b	100	2	1000	10	76	127	0.81	6.11	0.23	1.73	38
c	5	1	200	20	44	12	0.55	1.00	2.81	0.96	19

From (1.2), the group velocity, in the direction $\boldsymbol{e}_{\boldsymbol{k}}$ of $\boldsymbol{k}$, namely

$$\boldsymbol{v}_{\mathrm{g}}(\boldsymbol{k},\boldsymbol{r}) = \boldsymbol{\nabla}_{\boldsymbol{k}}\omega(\boldsymbol{k},\boldsymbol{r}) = \boldsymbol{e}_{\boldsymbol{k}}\sqrt{gh(\boldsymbol{r})}\left(1-\frac{1}{2}(h(\boldsymbol{r})k)^2+\cdots\right), \tag{1.3}$$

depends on k, and its maximum value corresponds to the speed $\sqrt{gh(\boldsymbol{r})}$ of the tsunami front. Behind the front are oscillations, representing wavenumbers k that have travelled more slowly. These waves intensify near the front, which can be regarded as a caustic (fold catastrophe; Poston & Stewart 1978; Nye 1999) in space–time. The result is the well-known Airy function tsunami profile (Jeffreys & Jeffreys 1956), whose principal feature is that the local 'wavelength', i.e. the distance between the first two wave crests (those closest to the front), after the tsunami has travelled a distance D, in a time t, is (Berry 2005; for some examples, see table 1)

$$\Lambda = 3.02(DH^2)^{1/3} = 3.02(vtH^2)^{1/3}. \tag{1.4}$$

The Airy theory can, at least in the case of constant depth, be extended (Berry 2005) to provide highly accurate uniform asymptotic approximations to the wave far from the front as well as close to it.

Second, underwater 'lenses' exhibit the two-dimensional analogue of spherical aberration (Born & Wolf 2005), so the typical effect of focusing is to concentrate the tsunami onto a cusped caustic (figure 1) rather than a focal point. 'Typical' is used here in the sense of singularity theory (Poston & Stewart 1978) to denote effects that are stable under perturbation: changing the profile of the underwater lens will shift the focus, but it will remain a cusp. Therefore, a focused tsunami is a caustic in space–time traversing a caustic fixed in space—a caustic on a caustic.

Third, the maximum group velocity occurs for $k=0$, so tsunami theory requires study of the long-wave limit, rather than the short-wave limit familiar in geometrical propagation and focusing effects. In the asymptotic theory presented here, the large parameter will be the distance from the lens to the focus divided by the local wavelength Λ of the tsunami; because of the long-wave nature of tsunami propagation, Λ increases with D (cf. (1.4)).

In tsunami focusing, these three characteristic effects—dispersion, the double singularity corresponding to a space–time fold caustic on a spatial cusped caustic, and long wavelengths—lead to an unusual wave profile described by an unfamiliar diffraction integral.

The plan of the paper is as follows. Section 2 describes the underwater lenses and the focusing they generate.

Section 3 gives the fundamental diffraction theory. Partially compensating the complications just described are two simplifying features. First, over most of its propagation range, the elevation of a tsunami wave (typically a metre or less) is much smaller than H (typically several kilometres), justifying the use of linear wave theory (Ward 2003); we do not consider shoaling, i.e. run-up on beaches, where the tsunami causes destruction and where the nonlinearity must be considered (Keller 1961; Keller & Keller 1964; Peregrine 1967). Second, close to the cusp the component plane waves $\boldsymbol{k}$ are travelling in almost the same direction, justifying the use of the paraxial approximation (Marcuse 1972; Goodman 1985).

Section 4 gives the main result of the paper, namely a formula for the profile of a typical tsunami wave as it travels through the focal cusp. The formula, incorporating the three complicating features described above, is a function of time, two coordinates on the water surface, and two parameters: one measures the distance from the lens to the cusped image (in units of Λ) and the other measures the spatial extent of the initial disturbance (also in units of Λ).

The most important consequence of focusing is amplification of the tsunami wave. Section 5 gives, as a quantitative measure, a formula for the surface elevation at the instant the tsunami front passes through the cusp divided by the elevation of the front in the absence of focusing (i.e. when the depth is constant). For realistic parameters, this amplification factor shows that a focused tsunami can be several times larger than an unfocused tsunami that has travelled the same distance. The transverse extent of strong focusing, also calculated in §5, can reach tens of kilometres.

In previous work, an asymptotic theory of focusing has been given (Dobrokhotov *et al.* 2006*a*,*b*), which neglects dispersion. Complementary to this is a theory (Berry 2005) that incorporates dispersion fully but neglects focusing. Numerical simulations of tsunami propagation (Lynett *et al.* 2003; Titov *et al.* 2005) automatically incorporate focusing effects but do not usually explore them in detail, and can also be regarded as complementary to the

analytical treatment given here. As explained at the end of §2, evidence of focusing can be seen in travel time maps of tsunamis in the Atlantic (Nirupama *et al.* 2006), Pacific (NOAA 2006) and Indian (Bhaskaran *et al.* 2005) Oceans, calculated from Huygens' principle and bathymetric data as a disturbance expanding at speed $\sqrt{gh(\boldsymbol{r})}$ from the source; as will be explained in §2, focusing is indicated by kinks (sharp bends) in the travel time contours.

2. Underwater tsunami lenses

Referring to figure 1, we consider a localized elevated region of seabed with height $f(\boldsymbol{r})$, which we will call a submerged 'island', rising smoothly from an ocean whose depth, far from the island, is the constant H. Thus, the ocean depth over the island is

$$h(\boldsymbol{r}) = H - f(\boldsymbol{r}), \tag{2.1}$$

and the refractive index, according to (1.1) is, for small f/H,

$$n(\boldsymbol{r}) = \sqrt{\frac{H}{H-f(\boldsymbol{r})}} \cong 1 + \frac{f(\boldsymbol{r})}{2H}. \tag{2.2}$$

Waves crossing the island in the x-direction experience a shift l in their 'optical distance', which can be expressed as a function of the transverse coordinate y_0 (figure 1) at the location $x{=}0$ of the island

$$l(y_0) = \int_{-\infty}^{\infty} \mathrm{d}x (n(x, y_0) - 1) \approx \frac{1}{2H} \int_{-\infty}^{\infty} \mathrm{d}x\, f(x, y_0). \tag{2.3}$$

The dominant focal behaviour depends on the small-y_0 behaviour, namely

$$l(y_0) = C - \frac{y_0^2}{2F_\mathrm{i}} + \frac{y_0^4}{4G^3} \ldots, \tag{2.4}$$

where F_i is the focal length of the island lens and the length G quantifies the aberration.

For definiteness, we consider an island modelled by the circular Gaussian

$$f(\boldsymbol{r}) = H_\mathrm{i} \exp\left(-\frac{r^2}{R^2}\right) \quad \text{and} \tag{2.5}$$

$$l(y_0) = \frac{H_\mathrm{i} R\sqrt{\pi}}{2H} \exp\left(-\frac{y_0^2}{R^2}\right). \tag{2.6}$$

Then

$$F_\mathrm{i} = \frac{HR}{H_\mathrm{i}\sqrt{\pi}}, \qquad G = \left(\frac{HR^3}{H_\mathrm{i}\sqrt{\pi}}\right)^{1/3} \quad \text{and} \quad C = \frac{H_\mathrm{i} R\sqrt{\pi}}{2H}. \tag{2.7}$$

If the island is at a distance D from the source of the tsunami (figure 1), it follows from the lens formula that the tsunami energy is focused at a distance

$$F = \frac{DF_\mathrm{i}}{D - F_\mathrm{i}} \tag{2.8}$$

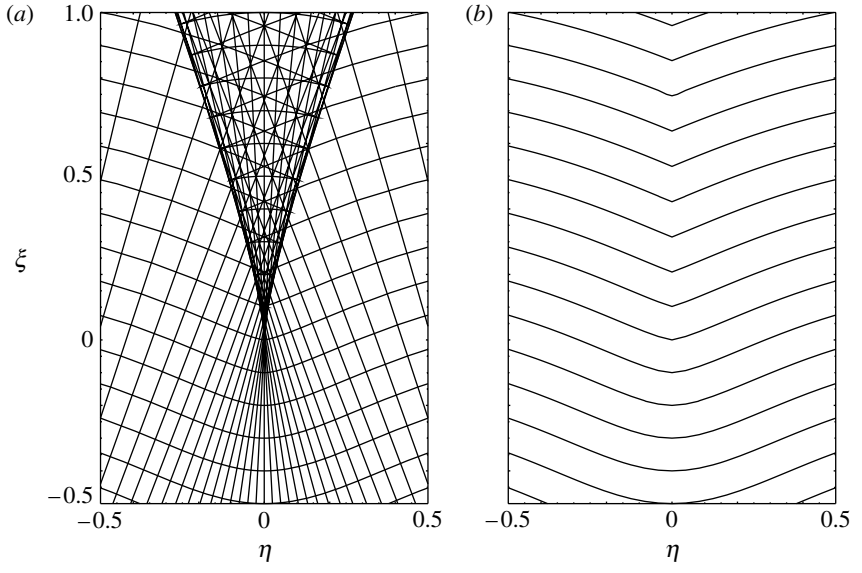

Figure 2. (*a*) Rays (2.11) (thin straight lines) enveloping a cusped caustic (2.13) and wavefronts (2.17), i.e. contours of travel time (bold curves). (*b*) Travel time contours as in (*a*), but showing only the first arrival.

from the lens. Some numerical examples of island lenses are given in table 1. There is no suggestion here that this circular Gaussian is a realistic model for underwater lenses; the expansion (2.4) is valid much more generally.

In terms of F, the optical distance to the point $\{x, y\}$ from $\{0, y_0\}$ is

$$d(y_0, x, y) = x + \frac{(y - y_0)^2}{2x} - \frac{y_0^2}{2F} + \frac{y_0^4}{4G^3} + \cdots. \tag{2.9}$$

It is convenient to use scaled coordinates, in which distances are measured in units of F, i.e.

$$\eta_0 \equiv y_0/F, \qquad \eta \equiv y/F, \qquad \xi \equiv x/F - 1, \qquad \gamma \equiv G/F. \tag{2.10}$$

The scaled geometrical aberration constant γ is of the order of unity; in the theory to follow, we will retain γ, but in numerical simulations we will set $\gamma = 1$. In scaled coordinates, the equation of the ray issuing from $\{0, \eta_0\}$ is, from $\partial d(y_0, x, y)/\partial y_0 = 0$ (Fermat–Hamilton principle of stationary optical distance),

$$\eta = -\eta_0 \xi + \frac{\eta_0^3(1 + \xi)}{\gamma^3}. \tag{2.11}$$

This family of straight rays is shown in figure 2*a*. As can be clearly seen, they envelop a cusped caustic.

The caustic is determined by $\partial^2 d(y_0, x, y)/\partial y_0^2 = 0$ (higher-order stationarity), i.e.

$$\eta_0^2 = \frac{\gamma^3 \xi}{3(1 + \xi)}, \tag{2.12}$$

from which elimination of η_0 using (2.11) gives the explicit form

$$\eta^2 = \frac{4}{27(1+\xi)}(\gamma\xi)^3. \tag{2.13}$$

The travel time contours, i.e. the 'wavefronts' giving the loci of points reached at times t, measured from the source event, by the tsunami travelling with speed $\sqrt{gh(\boldsymbol{r})}$, are defined by

$$t(x,\,y) = \frac{D + d(y_0, x,\, y)}{v} = t, \tag{2.14}$$

with y_0 determined by the ray equation. It is convenient to introduce the scaled time

$$\tau \equiv \frac{vt - D - F}{F}, \tag{2.15}$$

measured from the instant when the front crosses the focus. Then, (2.14) becomes

$$\tau(\eta_0, \xi, \eta) = \xi + \frac{\eta^2 - 2\eta\eta_0 - \xi\eta_0^2}{2(1+\xi)} + \frac{\eta_0^4}{4\gamma^3} = \tau, \tag{2.16}$$

with η_0 determined by the ray equation (2.11). In explicit parametric form, the contours are

$$\xi(\eta_0, \tau, \gamma) = \frac{4\tau\gamma^6 + 3\eta_0^4\gamma^3 - 2\eta_0^6}{2\big((2+\eta_0^2)\gamma^6 - 2\eta_0^4\gamma^3 + \eta_0^6\big)} \quad \text{and}$$

$$\eta(\eta_0, \tau, \gamma) = -\eta_0\xi(\eta_0, \tau, \gamma) + \frac{\eta_0^3(1 + \xi(\eta_0, \tau, \gamma))}{\gamma^3}. \tag{2.17}$$

For the important wavefront passing through the cusp, represented by $\tau = 0$, an explicit approximation, accurate for $|\eta| < 1$, is obtained from the leading-order behaviour of the above equation for $\eta(\eta_0, 0, \gamma)$, namely

$$\eta(\eta_0, 0, \gamma) \approx \frac{\eta_0^3}{\gamma^3}. \tag{2.18}$$

Thus, explicitly, the focal wavefront is

$$\xi(\eta) \approx \frac{3|\eta|^{4/3}\gamma - 2\eta^2}{2((2 + |\eta|^{2/3}) - 2|\eta|^{4/3}\gamma + \eta^2)}. \tag{2.19}$$

The fractional deviation of this approximation from the exact wavefront (2.17) vanishes at $\eta = 0$ and 1, and never exceeds 14%.

The travel time contours, calculated from (2.17), are shown in figure 2*a*, superimposed on the rays. Before the geometrical tsunami front encounters the cusped caustic, i.e. for $\tau < 0$, the contours are smooth. After the encounter, i.e. for $\tau > 0$, each contour possesses two cusps and one self-intersection, representing three successive arrivals of the geometrical front at points inside the cusp. The self-intersection represents two fronts that have travelled further, having passed by the side of the island; the third front has passed more slowly over the middle of the island and lags behind. In geometrical language (Arnold 1986),

the double-cusped wavefront is a swallowtail singularity of Legendre type in $\{\tau, \xi, \eta\}$ space, associated with the focal cusp, which is a singularity of Lagrange type in the $\{\xi, \eta\}$ plane.

In ocean travel time maps, the common practice is to include only the first arrival, as shown in figure 2*b* for the model lens considered here. The cusps are thereby eliminated, and focusing is indicated only by kinks in the travel time contours. Such kinks are common and visually obvious features of travel time maps. As an example from the Atlantic, fig. 7 of Nirupama *et al.* (2006) shows that a tsunami originating near Martinique, Caribbean, will be focused close to the Azores; in the Pacific, NOAA (2007) shows that a tsunami originating near the Kuril Islands, Russia, will be focused off the coast of Chile; and in the Indian Ocean, Bhaskaran *et al.* (2005) show that tsunamis originating near Indonesia will be focused close to the Kerguélen and Crozet Islands.

3. Paraxial theory of focused wave

Travel time maps, as shown in figure 2*a*, provide important practical information, by predicting when the tsunami will arrive at different places. But, even when extended to include the underlying rays and all arrivals associated with the caustic, they give only the most primitive indication of the structure of the tsunami wave. For a deeper understanding, it is necessary, in a phrase attributed to B Kinber, to 'sew the wave flesh on the geometrical bones'.

To achieve this, we begin by calculating the wave arriving at the underwater lens, as a superposition of plane waves $\boldsymbol{k}$ with different frequencies and directions, propagating from the source event at $t=0$. This will be represented by an initial ocean elevation $z(\boldsymbol{r}, 0)$ with total volume V and Fourier transform $\bar{z}(\boldsymbol{k})$, where $\bar{z}(\boldsymbol{0}) = 1$. For simplicity, we restrict ourselves to the case in which $z(\boldsymbol{r}, 0)$ has circular symmetry, and we also neglect the contribution to the tsunami from the initial distribution of water velocity; both restrictions can easily be relaxed. Then, standard theory (Ward 2003) gives the subsequent elevation as

$$z(\boldsymbol{r}, t) = \frac{V}{(2\pi)^2}\mathrm{Re}\int\!\!\int \mathrm{d}\boldsymbol{k}\, \bar{z}(\boldsymbol{k})\exp\{\mathrm{i}(\boldsymbol{k}\cdot\boldsymbol{r} - \omega(|\boldsymbol{k}|)t)\}$$

$$= \frac{V}{2\pi}\mathrm{Re}\int_0^\infty \mathrm{d}k\, k\bar{z}(k)J_0(kr)\exp\{-\mathrm{i}\omega(k)t\}. \tag{3.1}$$

As explained elsewhere (Berry 2005), for large distances r from the source, it is legitimate to replace the Bessel function J_0 by its asymptotic approximation, proportional to $\cos(kr-\pi/4)$, even though the tsunami wave profile is dominated by contributions from small k. Moreover, one of the two complex exponentials comprising the cosine can be neglected because its contribution to the integrand in (3.1) oscillates over the whole range of k and so cancels by destructive interference. Retaining the other exponential gives the elevation of the tsunami arriving at the lens as

$$z(r, t) = \frac{V}{\sqrt{8\pi^3 r}}\mathrm{Re}\left[\exp\left(-\frac{1}{4}\mathrm{i}\pi\right)\int_0^\infty \mathrm{d}k\, \sqrt{k}\bar{z}(k)\exp\{\mathrm{i}(kr-\omega(k)t)\}\right]. \tag{3.2}$$

With the cubic approximation (1.2) to $\omega(k)$, this integral (including the factor $\sqrt{k}$ reflecting the long-wave nature of tsunamis) can be evaluated approximately in terms of Airy functions (Berry 2005); we will not need the formula here, but note that it implies the local wavelength (1.4).

At the location of the lens, $r=\sqrt{D^2+y_0^2}\approx D+y_0^2/2D$. The lens impresses a y_0-dependent phase shift $kl(y_0)$ (cf. (2.3)) on the wave (3.2). Further paraxial propagation (Marcuse 1972) now gives the elevation of the focused tsunami at the point$\{x, y\}$ as a superposition of contributions from wavelets emanating from points $\{0, y_0\}$ as

$$z(x,y,t)=\frac{V}{4\pi^2\sqrt{Dx}}\mathrm{Re}\left[-\mathrm{i}\int_{-\infty}^{\infty}\mathrm{d}y_0\int_0^{\infty}\mathrm{d}k\,k\bar{z}(k)\exp\{\mathrm{i}(k(D+d(y_0,x,y))-\omega(k)t)\}\right], \tag{3.3}$$

where $d(y_0, x, y)$ is the optical distance (2.9).

A related application of diffraction theory to run-up on (non-submerged) islands is given by Kanoglu & Synolakis (1998).

4. Profile of focused tsunami wave

To proceed further, we model the initial disturbance by a Gaussian with radius W (not to be confused with the Gaussian underwater island (2.5) with radius R),

$$\bar{z}(k)=\exp\left(-\frac{1}{2}k^2W^2\right). \tag{4.1}$$

Then, with the cubic approximation (1.2), the integral over k in (3.3) can be evaluated exactly using

$$\begin{aligned}\int_{-\infty}^{\infty}\mathrm{d}u\,\mathrm{i}u\exp\left(\frac{1}{3}\mathrm{i}u^3-\frac{1}{2}Bu^2+\mathrm{i}Xu\right)\\ =2\pi\left[\frac{\partial}{\partial X}\exp\left(\frac{1}{12}B^3+\frac{1}{2}XB\right)\mathrm{Ai}\left(X+\frac{1}{4}B^2\right)\right].\end{aligned} \tag{4.2}$$

This exactness is a consequence of the Gaussian form, but accurate approximations, not given here, can be obtained for any initial disturbance.

It is convenient to employ the scalings (2.10) and (2.15) for the position and time variables and to define the parameters M and B by

$$\begin{aligned}M&\equiv\left(\frac{2}{H^2vt}\right)^{1/3},\qquad F\approx\left(\frac{2}{H^2(D+F)}\right)^{1/3}F\\ B&\equiv\frac{W^2M^2}{F^2}=\frac{W^2}{(H^2vt/2)^{2/3}},\end{aligned} \tag{4.3}$$

and the variable X by

$$X \equiv (\tau(\eta_0, \xi, \eta) - \tau)M = \left(\xi - \tau + \frac{1}{2(1+\xi)}\left(\eta^2 - 2\eta\eta_0 - \xi\eta_0^2\right) + \frac{\eta_0^4}{4\gamma^3}\right)M. \quad (4.4)$$

M is particularly important; it is the large asymptotic parameter of the theory, with the physical interpretation of being proportional to the focal distance from the lens divided by the local wavelength Λ (equation (1.4)) of the tsunami arriving at the lens. B is proportional to the radius of the source divided by Λ. Numerical examples are given in table 1.

Thus, the elevation becomes

$$z(x,\, y,\, t) = -\frac{V}{F^{3/2}\sqrt{D}}\, Z(\xi, \eta, \tau), \quad (4.5)$$

where

$$Z(\xi, \eta, \tau) \equiv -\frac{M^2}{4\pi\sqrt{1+\xi}} \exp\left(\frac{1}{12}B^3\right) \times \frac{\partial}{\partial X}\int_{-\infty}^{\infty} \mathrm{d}\eta_0 \exp\left(\frac{1}{2}BX\right) \mathrm{Ai}\left(X + \frac{1}{4}B^2\right). \quad (4.6)$$

The dependence on the parameters M, B and γ has not been indicated explicitly; actually, the number of parameters can be reduced from three to two by scaling, but the resulting expression is not very convenient. The formula (4.6) is the main result of this paper.

Since the wavefronts form a swallowtail singularity surface in $\{\tau, \xi, \eta\}$ space, it might be thought that the integral (4.6) is a swallowtail diffraction catastrophe (Berry & Upstill 1980; Nye 1999) in disguise, at least for $B=0$. But it is not, because the full caustic in $\{\tau, \xi, \eta\}$ space, obtained from the double integral (3.3), is the union of the swallowtail surface and the τ-independent cusp surface; alternatively stated, the exponent in the double integral over k and y_0 cannot be transformed into swallowtail form. However, the integral (4.6) can be evaluated numerically without difficulty, because of the fast convergence induced by the $+\eta_0^4$ term in X (equation (4.4)).

For each choice of the large parameter M and the source size parameter B, (4.5) gives the history of the tsunami, as it is being focused, in the variables $\{\xi, \eta, \tau\}$. Figure 3 shows the history, in the form of a series of snapshots, represented as density plots, for the case $M=10$, $B=0$, corresponding to a sharply localized initial disturbance. Figure 4 shows three-dimensional perspective views of the same wave. Before the focusing event, i.e. for $\tau<0$, the advancing front is followed by a series of the familiar Airy oscillations. For $\tau>0$, the oscillations are much stronger inside the cusped caustic curve, which is a locus of dislocated oscillations, i.e. the wave crests inside are continuous with the troughs outside. For larger M, and deeper within the cusp than is shown in figures 3 and 4, there is interference between the contributions associated with the three branches of the wavefront at each τ; the corresponding approximate form of (4.6), not given here, is a slowly beating superposition of three combinations of Airy functions.

Figures 5 and 6 are the corresponding pictures for $M=20$, $B=1$. The effect of the larger source B is to suppress the larger k contributions that generate the

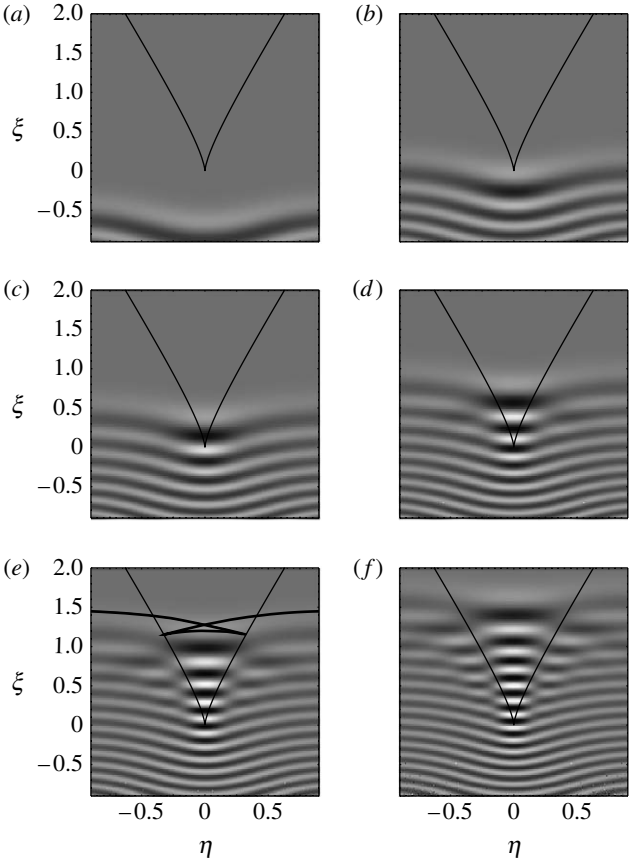

Figure 3. Density plots of tsunami height, represented by the function $Z(\xi, \eta, \tau)$, computed from (4.6) for $M=10$, $B=0$ for (*a*) $\tau=-0.6$, (*b*) $\tau=0$, (*c*) $\tau=0.4$, (*d*) $\tau=0.8$, (*e*) $\tau=1.2$ and (*f*) $\tau=1.6$. The caustic is indicated by the thin curves, and the thick curve in (*e*) is the geometrical wavefront.

oscillations following the front, so the tsunami is localized closer to the advancing front. The kinked wavefront inside the cusp (figure 2*a*) is clearly visible, especially in figure 5*e*.

As B increases further, the oscillations become weaker, and the tsunami profile (4.6) becomes a Gaussian-broadened wavefront traversing the caustic: one Gaussian outside and the superposition of three inside. Controlling this transformation is the asymptotic relation

$$\exp\left(\frac{1}{12}B^3+\frac{1}{2}BX\right)\mathrm{Ai}\left(X+\frac{1}{4}B^2\right)\underset{B\to\infty}{\to}\frac{1}{\sqrt{2B\pi}}\exp\left\{-\frac{X^2}{2B}\right\}. \tag{4.7}$$

This corresponds to the extreme long-wave limit in which dispersion is negligible, as can be confirmed directly from (3.3) after neglecting the cubic term in $\omega(k)$; it has been studied in detail by Dobrokhotov *et al.* (2006*a*,*b*).

A technical remark is that it might be thought that in (4.4) the factor $(1+\xi)$ in the denominator of one of the terms can be replaced by unity, since ξ is small near the focus. However, this replacement has the unphysical consequence that for larger ξ the tsunami is contaminated by causality-violating precursors,

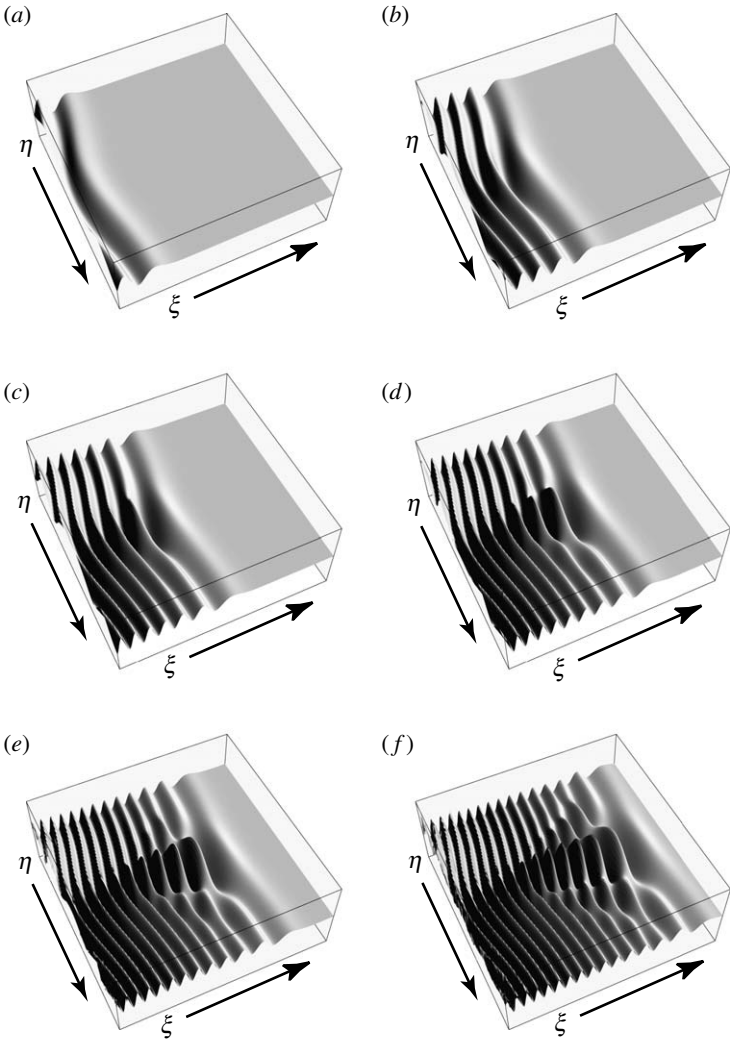

Figure 4. Three-dimensional views corresponding to figure 3.

arriving before the true initial front. By including the full factor $(1+\xi)$, incorporating the wave associated with the optical distance (2.4) exactly, causality is preserved.

5. Amplification at focus

A measure of the importance of the effect studied here is the elevation of the tsunami as it passes through the focus, i.e. $x=y=0$, $t=(D+F)/v$. From (4.4) and (4.5), this is

$$z_{\mathrm{foc}} \equiv z(0,0,(D+F)/v) = \frac{VM^{7/4}\gamma^{3/4}}{2\pi\sqrt{F^3D}}\, I_{\mathrm{foc}}(B), \tag{5.1}$$

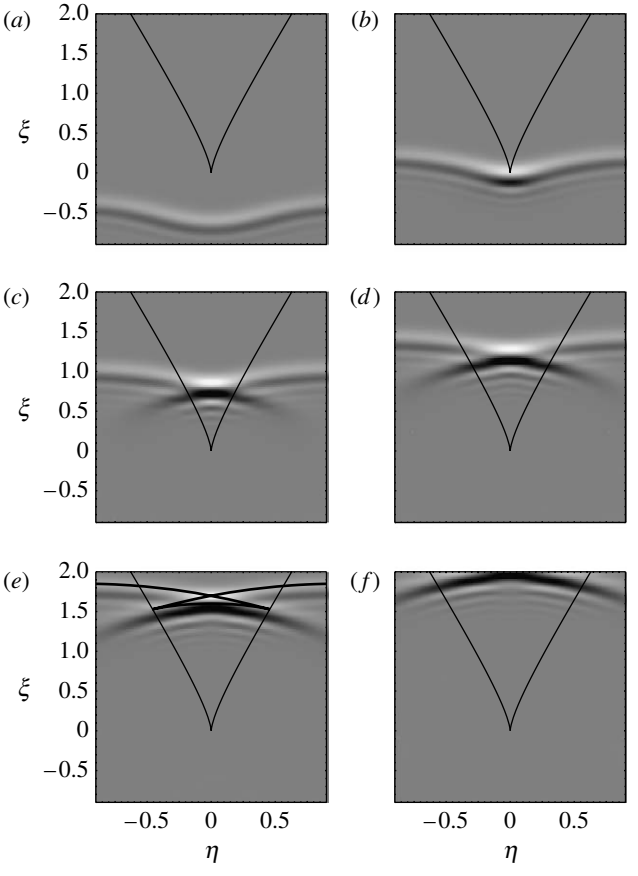

Figure 5. As figure 3, for $M=20$, $B=1$, (*a*) $\tau=-0.6$, (*b*) $\tau=0$, (*c*) $\tau=0.8$, (*d*) $\tau=1.2$, (*e*) $\tau=1.6$ and (*f*) $\tau=2.0$.

where

$$I_{\mathrm{foc}}(B) = -\exp\left(\frac{1}{12}B^3\right)\int_0^\infty \mathrm{d}s\,\exp\left(\frac{1}{8}Bs^4\right)\left[\mathrm{Ai}'\left(\frac{1}{4}(s^4+B^2)\right)\right.$$
$$\left.+\frac{1}{2}B\mathrm{Ai}\left(\frac{1}{4}(s^4+B^2)\right)\right]. \tag{5.2}$$

The focal elevation is the largest when $B=0$, i.e. for a concentrated source, and a calculation using the integral representation of the Airy functions gives

$$I_{\mathrm{foc}}(0) = \frac{\Gamma(1/4)}{2^{3/2}3^{5/12}\Gamma(5/12)} = 0.381201\ldots. \tag{5.3}$$

I_{foc} should be compared with the tsunami elevation at the corresponding event when there is no focusing, given by (3.2) evaluated at $r=vt=D+F$

$$z_{\mathrm{unfoc}} = \frac{VM^{3/2}}{\sqrt{8\pi^3F^3(D+F)}}I_{\mathrm{unfoc}}(B), \tag{5.4}$$

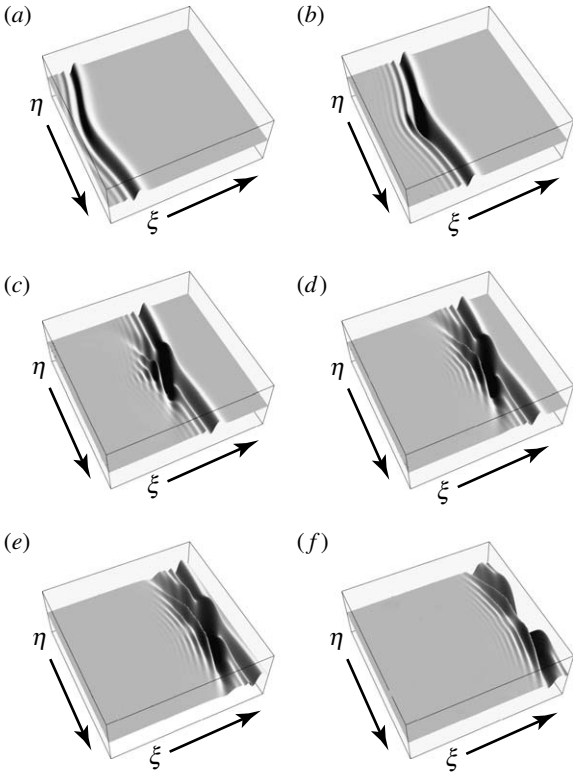

Figure 6. Three-dimensional views corresponding to figure 5.

where, after scaling the integration variable k in (3.2),

$$I_{\mathrm{unfoc}}(B) = \mathrm{Re}\left[\exp\left(-\frac{1}{4}\mathrm{i}\pi\right)\int_0^\infty \mathrm{d}\kappa\sqrt{\kappa}\exp\left(-\frac{1}{2}B\kappa^2 + \frac{1}{3}\mathrm{i}\kappa^3\right)\right]. \tag{5.5}$$

Again the largest value is for $B{=}0$ and an elementary calculation gives

$$I_{\mathrm{unfoc}}(0) = \sqrt{\frac{\pi}{3}}. \tag{5.6}$$

Including B, the amplification factor associated with focusing is therefore

$$A \equiv \frac{z_{\mathrm{foc}}}{z_{\mathrm{unfoc}}} = M^{1/4}\gamma^{3/4}\sqrt{1 + F/D}\; C\sigma(B), \tag{5.7}$$

where

$$C \equiv \sqrt{2\pi}\,\frac{I_{\mathrm{foc}}(0)}{I_{\mathrm{unfoc}}(0)} = 0.9337\ldots \quad \text{and} \quad \sigma(B) \equiv \frac{I_{\mathrm{foc}}(B)I_{\mathrm{unfoc}}(0)}{I_{\mathrm{unfoc}}(B)I_{\mathrm{foc}}(0)}. \tag{5.8}$$

Figure 7, showing $\sigma(B)$, indicates that the amplification gets smaller as the source gets bigger.

A consequence of the result (5.7) is that the amplification scales as $M^{1/4}$. The tsunami energy is proportional to the square of the surface elevation, so the amplification associated with focusing can represent a substantial increase

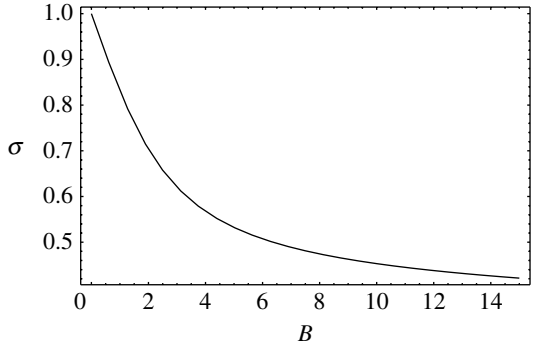

Figure 7. Tsunami amplification factor (5.7) and (5.8) at the focal event, as a function of the scaled source size B defined in (4.3).

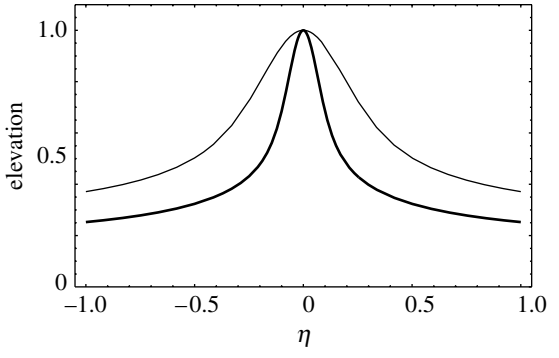

Figure 8. Tsunami elevation near the focal wavefront, showing transverse focusing enhancement. For each transverse position η, the maximum elevation is plotted for positions ξ close to the wavefront $\eta=0$, which passes through the cusp; this form of presentation is chosen because the maximum elevations occur for values of ξ slightly greater than those on the wavefront. Parameters are $M=10$ (thin curve) and $M=40$ (thick curve), $\gamma=1$, $B=0$; the pictures for $B=1$ are almost the same.

in destructive potential. Table 1 shows some numerical illustrations. In cases a and b, the focusing is a long-range effect and generates significant amplification because the parameter M is large, i.e. the focal distance F is much greater than the local wavelength Λ; in case a, the energy, proportional to A^2, is enhanced by a factor of the order of 10. In the shorter-range example c, Λ is larger than F, and there is no enhancement; in effect, the tsunami is scattered by the island, rather than being focused.

In view of the potentially serious practical implications of these focal enhancements, it is important to assess the transverse range over which focusing is significant. One possibility is to calculate the elevation on the focal wavefront at the crucial instant $\tau=0$. However, the maximum elevation occurs not exactly on this wavefront but close to it, and it is the maximum elevation at $\tau=0$ which is plotted in figure 8 (in fact, the pictures exactly on the wavefront are similar). As expected, the focal enhancement is restricted to a region, close to the cusp, that gets smaller as M increases.

For an estimate of the size of this region, we note that for points (ξ, η) on the wavefront, the argument (4.4) of the Airy function in (4.6) satisfies $X = \partial X/\partial\eta_0 = 0$. Therefore, in terms of the variable $\eta_1 \equiv \eta_0 - \eta_c$, where η_c is the stationary value of η_0 at the point on the wavefront being considered, expansion gives

$$X = M\left(\frac{1}{2}\left(\frac{3\eta_c^2}{\gamma^3} - \frac{\xi}{(1+\xi)}\right)\eta_1^2 + \frac{\eta_c}{\gamma^3}\eta_1^3 + \frac{1}{4\gamma^3}\eta_1^4\right). \tag{5.9}$$

On changing to the variable $u \equiv \eta_1 M^{1/4}/\gamma^{3/4}$, X becomes, close to the focus, i.e. for small ξ,

$$X = \frac{3}{2}u^2\alpha + u^3\alpha^{1/2} + \frac{1}{4}u^4, \tag{5.10}$$

where

$$\alpha \equiv \frac{M^{1/2}}{\gamma^{3/2}}\eta_c^2. \tag{5.11}$$

Strong focusing corresponds to dominance by the u^4 term, i.e. $\alpha < 1$, or after writing η_c in terms of the transverse variable η using (2.18),

$$\eta < \frac{1}{(M\gamma)^{3/4}}. \tag{5.12}$$

This is consistent with figure 8. In the original physical distance variables, the transverse extent of the region of strong focusing is

$$|y| < \Delta y = \frac{F}{(M\gamma)^{3/4}} = \left(\frac{HF(D+F)}{2\gamma^3}\right)^{1/4} \sim (F\Lambda^3)^{1/4}. \tag{5.13}$$

For the three cases in table 1, the distances Δy are given in the last column.

6. Concluding remarks

The results presented here suggest that focusing is a potentially serious effect that could make tsunamis more destructive where focal regions include sections of coasts. It would be useful to identify a locus of source locations for which this occurs, i.e. for which the cusp lies on a coastline. When the tsunami arrives at a coast, the focal amplification will be further amplified during run-up onto the beach—an important separate effect, not considered here, that has been much studied (Peregrine 1967; Tadepalli & Synolakis 1994; Tadepalli & Synolakis 1996; Kanoglu & Synolakis 1998).

For definiteness, a single circular Gaussian model island has been considered. Of course, as any modern atlas indicates, the topography of the floors of the oceans is much more complicated: underwater islands are not circular or isolated, there are underwater ridges, and depressions where the ocean is locally deeper. However, the main result (4.6) relies only on the tsunami front passing through a cusped focus, which is structurally stable against perturbations (Nye 1999), provided these are smooth.

Depressions ('anti-islands') on the ocean floor, which might be thought to act as defocusing lenses, can also generate cusped foci. An example is (2.5) with H_i negative; an elementary calculation reveals two cusps beyond the anti-island, on

either side. And even though the bottom profiles are not smooth, the effect of small irregularities is exponentially attenuated at the surface (Ward 2003). Small islands will cause weak scattering, and many of them will result in multiple scattering, but kinks on calculated travel time contours suggest that focusing, whose detailed profile has been calculated here, is the dominant effect.

I thank Prof. S. Dobrokhotov for helpful initial discussions; Prof. S. K. Dube for supplying the Tsunami Atlas for the Indian Ocean; the Physics Department of the Technion, Israel, for hospitality during drafting of this paper; and Prof. P. Shukla, Prof. J. H. Hannay and Prof. J. F. Nye and an anonymous referee for helpful comments.

References

Arnold, V. I. 1986 *Catastrophe theory*. Berlin, Germany: Springer.

Berry, M. V. 2005 Tsunami asymptotics. *New J. Phys.* **7**, 129. (doi:10.1088/1367-2630/7/1/129)

Berry, M. V. & Upstill, C. 1980 Catastrophe optics: morphologies of caustics and their diffraction patterns. *Prog. Optics* **18**, 257–346.

Bhaskaran, P. K., Dube, S. K., Murty, T. S., Gangopadhyay, A., Chaudhuri, A. & Rao, A. D. 2005 *Tsunami travel time charts for the Indian Ocean*. Kharagpur, India: Indian Institute of Technology.

Born, M. & Wolf, E. 2005 *Principles of optics*. London, UK: Pergamon.

Dobrokhotov, S. Y., Sekerzh-Zenkovich, S. Y., Tirozzi, B. & Volkov, B. 2006*a* Explicit asymptotics for tsunami waves in framework of the piston model. *Russ. J. Earth Sci.* **8**, 1–12. (doi:10.2205/2006ES000215)

Dobrokhotov, S. Y., Sekerzh-Zenkovich, S. Y., Tirozzi, B. & Tudorovskiy, T. Y. 2006*b* The description of tsunami waves propagation based on the Maslov canonical operator. *Dokl. Math.* **74**, 592–596. (doi:10.1134/S1064562406040326)

Goodman, J. W. 1985 *Statistical optics*. New York, NY: Wiley-Interscience.

Jeffreys, H. & Jeffreys, B. S. 1956 *Methods of mathematical physics*. Cambridge, UK: University Press.

Kanoglu, U. & Synolakis, C. E. 1998 Long wave runup on piecewise linear topographies. *J. Fluid Mech.* **374**, 1–28. (doi:10.1017/S0022112098002468)

Keller, J. B. 1961 Tsunamis—water waves produced by earthquakes. In *Tsunami hydrodynamics*, pp. 154–166, Monograph, no. 24, University of Hawaii, Hawaii: IUGG.

Keller, J. B. & Keller, H. B. 1964 Water-wave run-up on a beach. *ONR research report NONR-3828(00)*, pp. 1–40. Washington, DC: Department of the Navy.

Lamb, S. H. 1932 *Hydrodynamics*. Cambridge, UK: Cambridge University Press.

Lynett, P. J., Borrero, J. C., Liu, P. L.-F. & Synolakis, C. E. 2003 Field survey and numerical simulations: a review of the 1998 Papua New Guinea tsunami. *Pure Appl. Geophys.* **160**, 2119–2146. (doi:10.1007/s00024-003-2422-0)

Marcuse, D. 1972 *Light transmission optics*. New York, NY: Van Nostrand.

Nirupama, N., Nistor, I., Ponnambalam, K. & Murty, T. S. 2006 Tsunami travel time atlas for the Atlantic Ocean. *Mar. Geodesy* **29**, 179–199. (doi:10.1080/01490410600939231)

NOAA 2006 West Coast/Alaska Tsunami Warning Center tsunami travel time maps. See http://wcatwc.arh.noaa.gov/ttt/ttt.htm.

NOAA 2007 Tsunami originating in Kuril Islands, Russia. See http://wcatwc.arh.noaa.gov/ttvu529260-04.gif.

Nye, J. F. 1999 *Natural focusing and fine structure of light: caustics and wave dislocations*. Bristol, UK: Institute of Physics Publishing.

Peregrine, D. H. 1967 Long waves on a beach. *J. Fluid Mech.* **27**, 815–827. (doi:10.1017/S0022112067002605)

Poston, T. & Stewart, I. 1978 *Catastrophe theory and its applications*. London, UK: Pitman. (Reprinted by Dover 1996.)

Synolakis, C. E. & Bernard, E. N. 2006 Tsunami science before and after Boxing Day 2004. *Phil. Trans. R. Soc. A* **364**, 2231–2265. (doi:10.1098/rsta.2006.1824)

Tadepalli, S. & Synolakis, C. E. 1994 The run-up of *N*-waves on sloping beaches. *Proc. R. Soc. A* **445**, 99–112. (doi:10.1098/rspa.1994.0050)

Tadepalli, S. & Synolakis, C. E. 1996 Model for the leading waves of tsunamis. *Phys. Rev. Lett.* **77**, 2141–2144. (doi:10.1103/PhysRevLett.77.2141)

Titov, V., Rabinovich, A. B., Mojfeld, H. O., Thomson, R. E. & Gonzalez, F. I. 2005 The global reach of the 26 December 2004 Sumatra tsunami. *Science* **309**, 2045–2048. (doi:10.1126/science.1114576)

Ward, S. N. 2003 Classical tsunami theory—a la Ward. See http://es.ucsc.edu/~ward/papers/papers_index.htm.